Acta Crystallographica Section D
Biological Crystallography
ISSN 0907-4449

High-resolution diffracting crystals of intrinsically active p38α MAP kinase: a case study for low-throughput approaches

Ron Diskin,[a] David Engelberg[b] and Oded Livnah[a]*

[a]The Wolfson Centre for Applied Structural Biology, The Silberman Institute of Life Sciences, The Hebrew University of Jerusalem, Givat Ram, Jerusalem 91904, Israel, and [b]Department of Biological Chemistry, The Hebrew University of Jerusalem, Givat Ram, Jerusalem 91904, Israel

Correspondence e-mail: oded.livnah@huji.ac.il

Received 15 September 2006
Accepted 16 October 2006

p38 MAP kinases are central signalling molecules that mediate cellular responses to numerous environmental conditions and signalling molecules. Their proper function is required for many processes, including stress response, apoptosis, differentiation, growth and even learning and memory. Abnormal activity of p38 MAP kinases is associated with the aetiology of many diseases, making understanding their activation mechanisms highly critical. In this respect, mechanistic insights may be derived from structural studies of recently developed intrinsically active p38α mutants. Unlike wild-type p38α, which routinely crystallized, the active mutants caused severe difficulties during the crystallization process. The main hindrance was found to be protein heterogeneity, which was meticulously resolved by genetically modifying the recombinant protein and optimizing the expression and purification protocols. The success in obtaining crystallizable proteins strongly emphasizes that in certain cases, high-throughput techniques (crystallization robots) together with low-throughput approaches, with careful monitoring and analysis of the results, are essential.

1. Introduction

p38 mitogen-activated protein (MAP) kinases are serine/threonine kinases that are expressed in all eukaryotic cells and are activated in response to a variety of stimuli. Normal function of p38 is essential for both cellular and multicellular processes (Zarubin & Han, 2005; Ono & Han, 2000), whereas abnormal p38 activity is associated with various diseases, including chronic inflammatory diseases, psoriasis, myocardial injuries and cancer (Engelberg, 2004; Lee *et al.*, 2000). There are four p38 isoforms (α, β, γ and δ) which belong to the MAP kinase superfamily, which also includes the extracellular signal-regulated kinases (ERKs), the c-Jun N-terminal kinases (JNKs/SAPK) and the big MAP kinases (BMKs/ERK5 and ERK7; Cano & Mahadevan, 1995; Ono & Han, 2000). All MAP kinases share the same basic activation mechanism (Songyang *et al.*, 1996) and are characterized by a common activation motif composed of a Thr-*X*-Tyr sequence located on a flexible loop termed the phosphorylation lip. In response to an appropriate stimulus, the corresponding threonine and tyrosine are phosphorylated by dual-specificity kinases termed MAP kinase kinases (MAPKKs or MKKs). This dual phosphorylation consequently renders the enzymes catalytically active. Conversely, unphosphorylated MAP kinases exhibit negligible activity levels (Robbins *et al.*, 1993; Cobb & Goldsmith, 2000; Canagarajah *et al.*, 1997).

Recently, we have designed and constructed the first series of intrinsically active p38 MAP kinases p38α and p38γ (Diskin *et al.*, 2004) and subsequently p38β and p38δ (Avitzour *et al.*, 2007). These molecules are spontaneously active and independent of MAPKK activation both *in vitro* (as recombinant purified proteins) and *in vivo* (in cell cultures; Askari *et al.*, 2007). In addition, biochemical studies revealed that the activation mechanism of the p38α mutants involves trans-autophosphorylation on their phosphorylation lip and subsequent activation (Diskin *et al.*, 2007). The biochemical data derived from the bioassays were extremely intriguing, which made the intrinsically active mutants attractive targets for structural studies.

Table 1
Data-collection statistics.

Values in parentheses are for the outer resolution shell.

p38α mutant	D176A+F327L	D176A	D176A+F327S form *A*	D176A+F327S form *B*
ESRF beamline	ID14-4	ID14-3	ID29	ID29
Wavelength (Å)	0.925	0.931	0.953	0.979
Detector	ADSC Quantum 4R CCD	MAR 165 CCD	ADSC Quantum 315R CCD	ADSC Quantum 315R CCD
Data-collection temperature (K)	100	100	100	100
Space group	$P2_12_12_1$	$P2_12_12_1$	$P2_12_12_1$	$P2_12_12_1$
Unit-cell parameters (Å)	a = 68.67, b = 69.79, c = 74.22	a = 67.86, b = 69.42, c = 74.06	a = 68.00, b = 69.68, c = 74.49	a = 68.93, b = 74.59, c = 74.13
Resolution range (Å)	40–1.45 (1.5–1.45)	50–1.83 (1.86–1.83)	48.8–1.70 (1.76–1.70)	31.2–1.86 (1.82–1.85)
Unique reflections	63600	29662	39403	32410
Redundancy	7.8	5.0	14.1	5.3
$R_{sym}(I)$†	5.5 (66.8)	8.8 (39.1)	7.2 (44.2)	5.7 (66.8)
Completeness	99.4 (100.0)	99.1 (95.3)	99.7 (98.2)	99.1 (99.9)
$I/\sigma(I)$	46.1 (3.1)	22.0 (1.9)	75.9 (5.8)	45.8 (3.0)
PDB code	2fst	2fso	2fsl	2fsm

† $R_{sym}(I) = \sum |I - \langle I \rangle| / \sum I$.

A highly homogeneous protein solution is a fundamental requirement for crystallization (Durbin & Feher, 1996). This parameter is extremely important both for nucleation and crystal growth (Durbin & Feher, 1996). Nonhomogeneous protein preparation could result from protein impurities that are present owing to an inadequate purification protocol or proteolytic degradation. Other types of heterogeneity which could impair crystallization include multiple protein conformations and post-translational modifications such as glycosylation, phosphorylation and methylation. Several of the heterogeneity-determining factors could be eliminated by employing different purification procedures. The effects of other factors, however, are more difficult to reduce and require different alterations in the protein-expression stages.

In this study, we describe our laborious efforts to obtain well diffracting crystals of three intrinsically active p38α mutants. For this purpose, we have performed several crucial modifications of both the expression protocol and the protein sequence in order to eliminate protein heterogeneity. We have used a feedback mechanism where we preformed an automated crystallization screen after each stage of modifying the protein. Only after resolving the problem and obtaining highly homogeneous protein were we able to optimize the crystallization conditions and obtain well diffracting crystals. Our findings are of general interest to the field of protein crystallization in terms of analyzing the factors that induce protein heterogeneity and consequently resolving them. Such an approach could be employed in 'difficult' crystallization projects and combined with the modern high-throughput notion of automatically screening a vast number of conditions. In this context, it is more fruitful to step back and thoroughly analyze the factors that impair crystallization and resolve them successfully *via* feedback of information and low-throughput approaches.

2. Material and methods

2.1. Subcloning of p38α active mutants

We used the polymerase chain reaction (PCR) to produce a short His tag fused to the p38α gene. We introduced a sequence of six histidine residues in frame with the N-terminus of p38α using two primers: 5′-AATAACCATGGCGCATCATCATCATCATCATTCTCAGGAGAGGCCCACGTTCTACCG and 5′-ATTGGATCCTCAGGACTCCATCTCTTCTTGGTC. The PCR products were digested with *Nco*I and *Bam*HI endonucleases and ligated to *Nco*I/*Bam*HI-digested pET-28a (Novagen).

2.2. Expression of p38α active mutants

The vector plasmids containing the p38α genes were introduced into the Rosetta strain of *Escherichia coli* (Novagen). An overnight 25 ml starter culture was inoculated into 1.5 l fresh Luria–Broth (LB) medium containing ampicillin, grown at 310 K to an OD_{600} of 0.4 and transferred to 294 K for 30 min. Protein expression was obtained by supplementing the medium with 0.2 m*M* isopropyl β-D-thiogalactopyranoside (IPTG) for 5 h. The cells were collected by centrifugation and stored at 253 K.

2.3. Purification of p38α active mutants

Cell pellets were gently thawed on ice and suspended in a cold buffer containing 0.5 *M* NaCl, 50 m*M* Tris–HCl buffer pH 7.4, 10 m*M* imidazole (buffer *A*) supplemented with protease-inhibitor cocktail (Sigma) and disrupted mechanically using a microfluidizer (model M-110 EHIS, Microfluidics Corp., Newton, MA, USA). The soluble and insoluble phases were separated by centrifugation (40 000*g* for 50 min). The supernatant was loaded onto a 7 ml Ni^{2+}-chelating Sepharose column (Amersham) pre-equilibrated with buffer *A*. The bound protein was extensively washed and eluted using a linear gradient of imidazole in buffer *A*. The protein-containing fractions were pooled and dialyzed against 100 m*M* NaCl, 25 m*M* Tris–HCl pH 7.4, 1 m*M* ethylenediaminetetraacetic acid (EDTA) for several hours. The protein was further dialyzed against 100 m*M* NaCl, 25 m*M* Tris–HCl pH 7.4, 10 m*M* $MgCl_2$, 1 m*M* dithiothreitol (DTT). Subsequently, the protein was loaded on a Source 15Q anion-exchange column (Amersham) equilibrated with 100 m*M* NaCl, 50 m*M* Tris–HCl pH 7.4, 5% glycerol, 10 m*M* $MgCl_2$, 1 m*M* DTT and eluted using a linear gradient of NaCl in the same buffer. The fractions containing the protein were pooled and subjected to a second consecutive purification using the Source 15Q column. Purified protein was diluted in a 1:1 ratio with 10 m*M* DTT, 10 m*M* $MgCl_2$, 5% glycerol and concentrated using Vivaspin (VivaScience) to 14 mg ml^{-1} (determined by absorption at 280 nm) and stored at 193 K.

2.4. Crystallization

Crystals were obtained for all mutants using the sitting-drop vapour-diffusion method at 293 K with a reservoir solution containing 10–15% PEG 3350, 100 m*M* HEPES pH 7.25, 200 m*M* KF, 25 m*M* *n*-octyl β-D-glucopyranoside (β-OG). The thin plate-shaped crystals reached their final dimensions within 2–3 d but were unsuitable for crystallographic analysis. Crystals were further

enlarged by streak-seeding (Stura & Wilson, 1991) and subsequent incubation at 277 K to dimensions of 0.3 × 0.3 × 1.0 mm within 7–9 d. All mutant crystals were cryoprotected in Paratone-N oil and immediately flash-cooled to 100 K for diffraction data collection.

2.5. Data collection and refinement

Crystallographic data for p38$\alpha^{D176A+F327L}$, p38$\alpha^{D176A+F327S}$ (two crystal forms) and p38α^{D176A} were collected at the European Synchrotron Radiation Facility (ESRF). Data for all crystals were integrated and scaled using the *HKL* suite (Otwinowski & Minor, 1997). The crystals of the three p38α mutants belonged to the orthorhombic space group $P2_12_12_1$, with one molecule in the asymmetric unit (Table 1).

The structures of the p38α mutants were solved *via* molecular-replacement methods using *MOLREP* (Vagin & Isupov, 2001) implemented in *CCP*4 using the atomic coordinates of p38α (PDB code 1wfc; Wilson *et al.*, 1996) as the initial search model after removing all solvent molecules. The structures were refined using *REFMAC*5 (Murshudov *et al.*, 1997) and solvent molecules were added using *ARP*/*wARP* (Morris *et al.*, 2003). The structures were fitted into electron-density maps using the graphics program *O* (Jones *et al.*, 1991). The atomic coordinates have been deposited and are available (Table 1) from the RCSB Protein Data Bank (Berman *et al.*, 2002).

3. Results

3.1. Initial crystallization trials of p38α

The crystal structures of human and murine wild-type p38 (p38α^{wt}) became available in the late 1990s (Wilson *et al.*, 1996; Wang *et al.*, 1997). The two proteins are virtually identical in sequence and function, differing by only one amino-acid residue in a nonfunctional location. Currently, there are approximately 40 available p38α structures, of which most are complexes with various inhibitors and peptides. The recombinant protein used for crystallization of human p38α^{wt} was produced in SF9 insect cells (Wilson *et al.*, 1996), whereas the murine protein was produced in BL21 *E. coli* cells (Wang *et al.*, 1997). The purification procedures of these two proteins differ substantially; the purification procedure of the murine protein was somewhat simpler than that reported for the human p38α (Fig. 1). In most cases reported to date, the selected conditions for protein expression and purification were similar to the simpler murine p38α production.

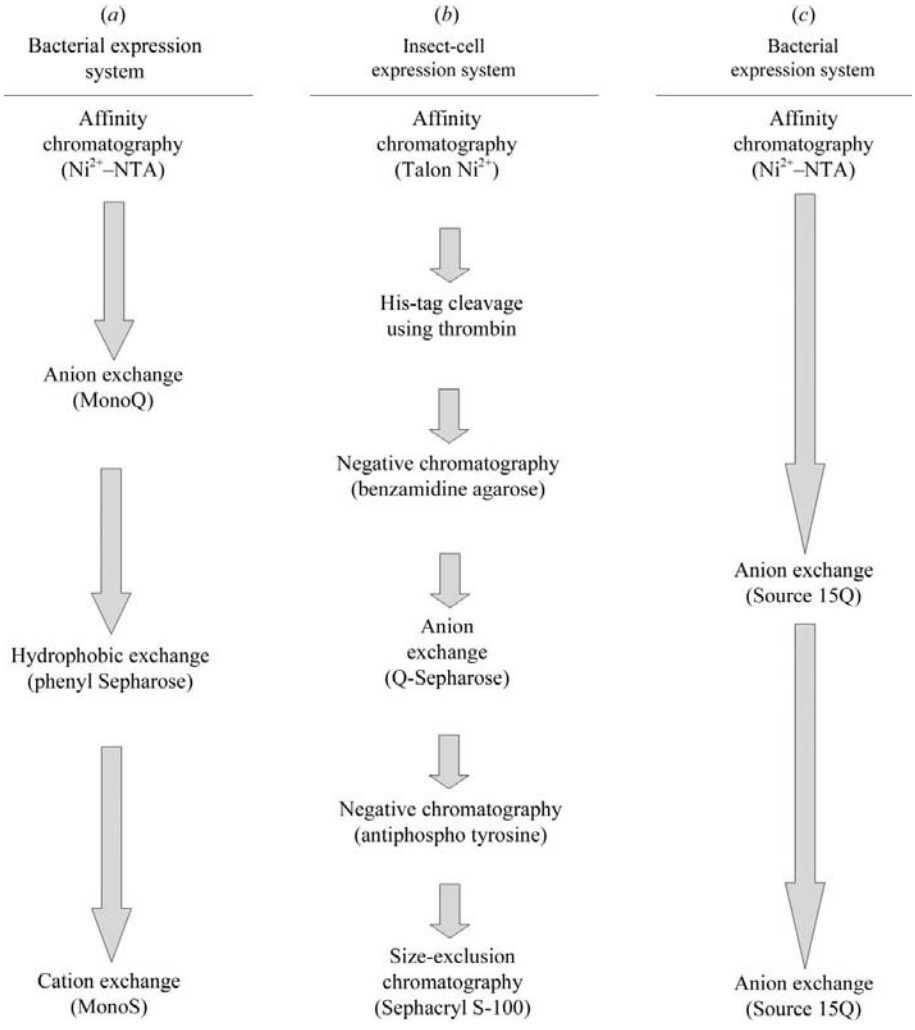

Figure 1
Schematic summary of the purification protocols used for p38α. The flowcharts illustrate (*a*) the purification strategy employed by Wang *et al.* (1997) for murine p38α, where four purification steps were employed. (*b*) A more extensive six-step purification was utilized for human p38α expressed in insect cells as described by Wilson *et al.* (1996). The purification protocol of the active human p38α mutants included only three steps (*c*).

We gained substantial experience in expressing intrinsically active p38α mutants in *E. coli* (Diskin *et al.*, 2004), reaching an average yield of approximately 70 mg of soluble p38α mutant per litre of bacterial culture. In order to purify the protein for crystallization purposes, we initially elected to follow the simpler murine protein-purification strategy (Fig. 1). We observed that the mutants did not bind to the MonoS column as reported and we thus replaced this purification step by size-exclusion chromatography (Superdex 75). Using this procedure, we were able to obtain highly homogeneous protein solution. The protein eluted in a single symmetrical peak from the Superdex column and appeared as a single band in SDS–PAGE with Coomassie staining. Consequently, we attempted to crystallize the intrinsically active p38α mutants by initially using the previously reported crystallization conditions (Wilson *et al.*, 1996; Wang *et al.*, 1997) and also screening for alternative conditions using a crystallization robot. Unfortunately, we were unable to reproduce the reported success in crystallization of human and murine p38. This lack of crystallization success prompted us to investigate further.

3.2. The heterogeneous phosphorylation pattern

Protein analysis using SDS–PAGE and gel-filtration chromatography failed to reveal that the expressed p38 active variants in fact consisted of several forms with different levels of phosphorylation. We

become aware of the diverse phosphorylation pattern by using a phospho-specific dye (ProQ-Diamond molecular probes) which stained the protein. High-resolution anion-exchange chromatography using a custom HR 16/10 column packed with Source-15Q resin (Amersham) showed the possible presence of different peaks (Fig. 2*a*), indicating a different pattern of charges on the protein surface. However, the separation was insufficient to obtain a single charged species. Western blot analysis using three specific antiphospho antibodies revealed that the fractionated protein is characterized by different phosphorylation patterns (Fig. 2*b*). We have used anti-P-p38 antibody (cell signalling) that can specifically identify phosphorylation on the unique activation motif of p38α, as well as antibodies that can detect phosphorylation on threonine and tyrosine residues. All the fractionated protein stained positively for the existence of phospho-Thr, which was probably in the activation motif. Some of the fractions contained phospho-Tyr, especially a minor proteolytic product that was not noticeable by Coomassie staining. We inferred and later verified that this phosphorylation results from trans-autophosphorylation activity and is part of the activation mechanism of the active mutants (Diskin *et al.*, 2007).

As the expressed active p38α variants were shown to be heterogeneously phosphorylated, we initiated an effort to substantially reduce the extent of phosphorylation or abolish it completely. Initially, we examined the influence of the protein induction time. We assumed that the long inductions (*i.e.* 12 h) we were using to obtain large amounts of protein ($\sim$70 mg l^{-1}) resulted in a high concentration of p38α allowing sufficient time for phosphorylation to occur in bacterial cells. Using shorter induction times, we were able to lower the level of phosphorylation (determined using ProQ staining and anion-exchange chromatography) and increase the homogeneity of the p38α, while consequently reducing the yield. The second parameter that was examined was the induction temperature. We have discovered that when using a relatively low induction temperature (294 K in comparison to 305 K) phosphorylation is almost completely prevented. Combining a short 5 h induction with a low expression temperature (294 K) resulted in highly homogeneous unphosphorylated protein (Fig. 3*a*), which eluted from the anion-exchange column as a single peak (Fig. 3*b*).

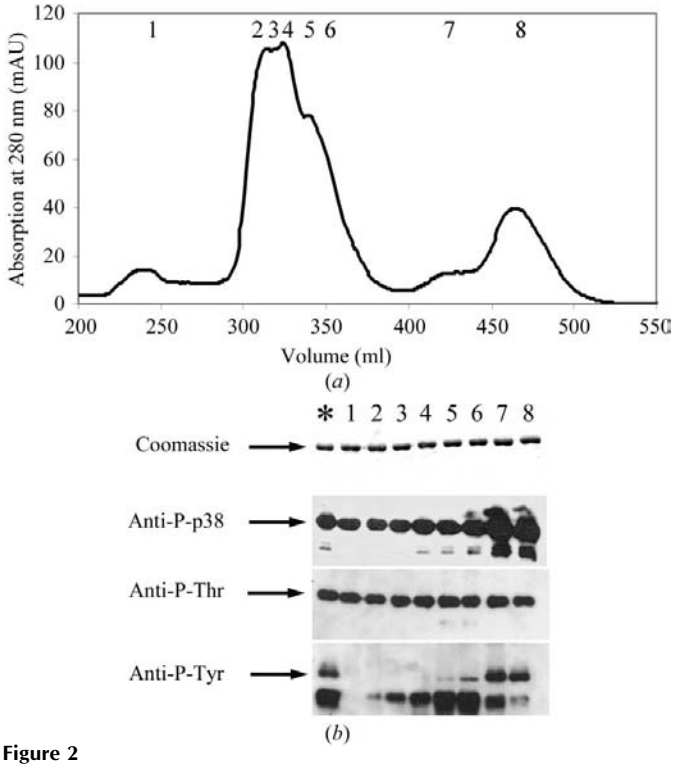

Figure 2
At high temperature, p38α is phosphorylated. (*a*) Anion-exchange chromatogram of p38α mutant expressed at 305 K depicting the absorption at 280 nm *versus* elution volume. Protein was bound to Source 15Q resin and eluted with a linear increasing gradient of NaCl. The numbers indicate the fractions that were collected and used for Western blot analysis. (*b*) Western blot analysis using antiphospho antibodies. Arrows indicate the migration of p38α. Coomassie staining indicates the total amount of protein in each lane. Three different antiphospho antibodies were used to analyze the phosphorylation pattern of the various protein fractions. An asterisk specifies the protein pool prior to fractionation using anion-exchange chromatography. Numbers indicate the fractions used for analysis according to Fig. 2(*a*).

3.3. Optimization of the expression construct

The N-terminal segment of p38α is disordered to some extent in all known p38α crystal structures. In this context, the first residue in most reported p38α structures is Arg5. When expressing a recombinant protein in heterologous system, a His tag is often added to the protein for affinity-purification purposes (Fig. 1). The recombinant His tag derived from the pET15 expression plasmid (Novagen) adds 25 amino acids (Fig. 4) to the protein, including six histidines followed by a thrombin cleavage site. We were thus concerned whether the conformational freedom of this long recombinant tag may interfere with crystallization. The effect of the composition and the length of recombinant fusion tags on protein crystallization and diffraction quality has previously been observed and reported (Bucher *et al.*, 2002). In addition, we were concerned that the recombinant His tag

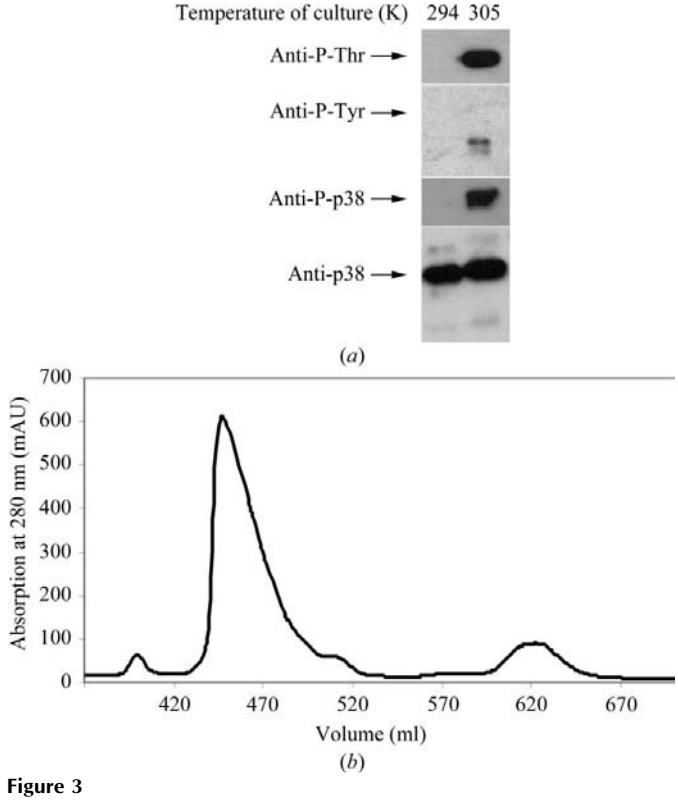

Figure 3
At low temperature, p38α is not phosphorylated. (*a*) Phosphorylation-pattern comparison between proteins expressed at 294 and 305 K. In this analysis, we used the same three antiphospho antibodies used in Fig. 2(*b*). In addition, we have used anti-p38 antibody to assess the amount of protein in each lane. (*b*) Anion-exchange chromatogram of the p38α mutant expressed at 294 K. The chromatogram shows absorption at 280 nm *versus* elution volume under conditions similar to those described in Fig. 2(*a*).

could introduce additional heterogeneity into the protein. It has previously been shown that serine residues in recombinant His tags attached to protein kinases serve as nonspecific phosphorylation sites, leading to heterogeneity and functional abnormalities (Du *et al.*, 2005). Furthermore, a short His tag fused to p38α^{wt} has been reported to have been successfully purified and crystallized (Bukhtiyarova *et al.*, 2004). We thus constructed an expression vector to produce our intrinsic active p38α mutants fused to a minimal His tag composed of only eight additional amino-acid residues (Fig. 4).

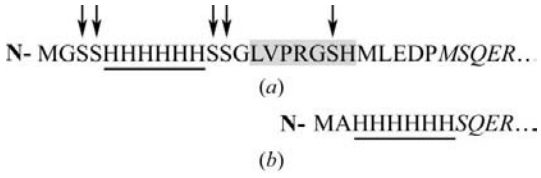

Figure 4
The recombinant N-terminal fusion His tags. (*a*) The 25-amino-acid His tag derived from pET15 and (*b*) the shorter His tag used in this study. The six histidines are underlined and italics indicate the first amino acids of p38α. The thrombin-cleavage site is highlighted in light grey and the serine residues that are potential nonspecific phosphorylated sites are indicated by arrows.

As a mode of operation, we conducted automated crystallization assays using a robot after each protein-modification stage described above. Only after the two stages of eliminating the phosphorylation of the protein and shortening the His-tag spacer did we obtain initial crystallization results.

3.4. Crystallization of p38α active mutants

We initially selected the double mutant p38$\alpha^{D176A+F327L}$ for crystallization attempts as it is one of the two most active p38α mutants (Diskin *et al.*, 2004). We established a modified purification strategy (Fig. 1) based on our experience with high-resolution anion-exchange chromatography. The initial results were obtained from a crystallization screen (Crystal Screen, Hampton Research) set up using an Oryx-6 (Douglas Instruments) crystallization robot with the microbatch method. The experiments were set up on hydrophilic 96-well Vapor Batch plates (Hampton) and covered with paraffin/silicon oil (75:25) at a temperature of 293 K. We were able to obtain very small spheroids on the skin that formed in the 2 µl crystallization drop using PEG 6000 as a precipitant with Tris–HCl pH 8.0 in the crystallization solution (Fig. 5*a*). Screening for better crystallization conditions initially resulted in larger spheroids (Fig. 5*b*; PEG 3350, KF) and, by adding octyl β-D-galactopyranoside (β-OG), in needle-shaped crystals (Figs. 5*c*, 5*d* and 5*e*). We could not optimize the crystallization results any further using the microbatch method. We then utilized the sitting-drop vapour-diffusion method (without using the crystallization robot), resulting in spherical crystal clusters composed of thin plates (Figs. 5*f* and 5*g*). Fine adjustments of pH value and other parameters such as concentrations of the precipitating agent, salt and protein solution resulted in the formation of single thin plate-shaped crystals (Fig. 5*h*). The 6 µl crystallization drop contained a 1:1 protein solution:reservoir mixture. The protein solution was composed of 14 mg ml^{-1} protein, 5 m*M* dithiothreitol (DTT), 5% glycerol, 10 m*M* $MgCl_2$, 100 m*M* NaCl and the reservoir was composed of 15% PEG 3350, 100 m*M* HEPES pH 7.25, 200 m*M* KF, 25 m*M* β-OG. Better (thicker) crystals were not obtained by further screening for crystallization conditions. In order to obtain suitable crystals for diffraction experiments, we used the microseeding streak-seeding technique with a cat whisker (Stura & Wilson, 1991) using the thin plate-like crystals as the source of microseeds. The nuclei were seeded into 12 h pre-equilibrated sitting-drop experiments at 277 K (containing the same crystallization solution as indicated above). Crystals of p38$\alpha^{D176A+F327L}$ suitable for X-ray analysis appeared after 24 h and grew to their final dimensions within 7–9 d (Fig. 5*i*). It should be noted that without the streak-seeding procedure crystals did not appear spontaneously at 277 K. Furthermore, applying similar streak-seeding techniques at 293 K

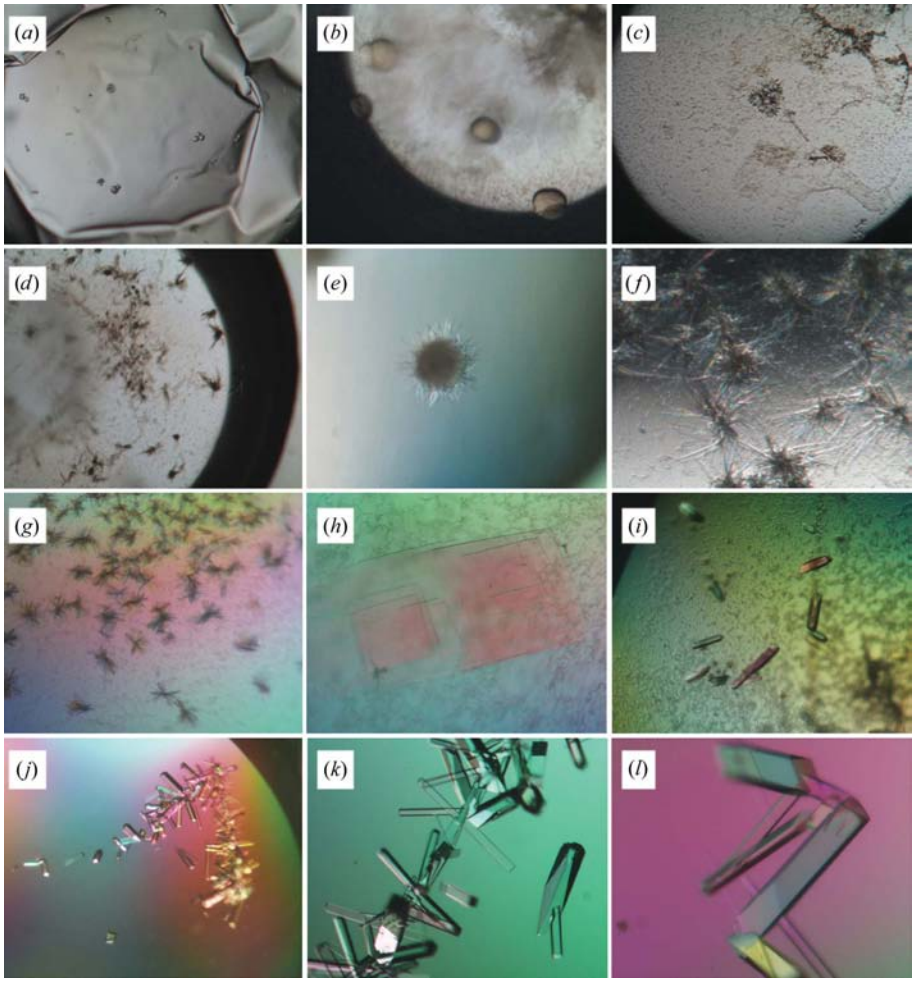

Figure 5
The crystallization progress of the p38$\alpha^{D176A+F327L}$ active mutant. The protein first crystallized as small spheroids (*a*, *b*). After initial optimization, clusters of fine needles were obtained (*d*) and evolved into thin plates after further optimization (*e*, *f*, *g*). Larger multiple thin crystals were then obtained (*h*) and were used as the source of microcrystals that were then streak-seeded to produce crystals suitable for X-ray analysis (*i*, *j*, *k*, *l*), which reached final dimensions of 0.3 × 0.3 × 1.0 mm (*l*).

reproduced the plate-like crystals. The three-dimensional crystals become a source for better crystal nuclei and allowed us enlarge the crystals (Figs. 5*j*, 5*k* and 5*l*).

We applied a similar approach as described above to obtain crystals of the two other active p38α mutants (*i.e.* p38α^{D176A}, and p38$\alpha^{D176A+F327S}$). We assumed that the overall topologies of these mutants do not differ greatly from that of the p38$\alpha^{D176A+F327L}$ mutant and that similar crystal packing could be formed. However, as crystals of the p38α^{D176A} and p38$\alpha^{D176A+F327S}$ mutants did not appear spontaneously, we applied cross-seeding approaches using crystals of p38$\alpha^{D176A+F327L}$ as the source of microseeds (Stura *et al.*, 1992). This procedure resulted in crystals of the other two mutants suitable for X-ray analysis.

3.5. Data collection

Numerous cryoprotectant solutions (containing various concentrations of glycerol, ethylene glycol, xylitol, sucrose, light PEGs *etc.*) based on the crystallization conditions of the p38α active mutants were screened for collection of data at low temperatures, but in all cases the crystals disintegrated or dissolved soon after transfer. In an attempt to overcome this problem, we included 5–10% glycerol in the crystallization solution and subsequently obtained similar crystals of the proteins to those described above (Fig. 5). Unfortunately, the glycerol-grown crystals did not freeze well and did not tolerate transfer into cryoprotectant solutions. In order to collect crystallographic data at cryotemperatures, we briefly transferred the crystals into Paratone-N oil and then mounted them on a cryoloop. The cryocooled crystals exhibited relatively high mosaicity (2–3°). Lower mosaicity could be attained by mounting the crystals at 277 K (the temperature of growth) and cryo-screening for the lowest mosaicity, which reached a minimal value of ∼0.4°. Crystallographic data for the three p38α active mutants were collected at the European Synchrotron Radiation facility (ESRF) at different beamlines as indicated in Table 1. We were able to collect full data sets and to solve the structures of all three mutants at relatively high resolutions (Diskin *et al.*, 2007). Moreover, the structure of p38$\alpha^{D176A+F327L}$ was determined at 1.45 Å resolution, which is the highest reported resolution of a MAP kinase to date. The diffraction and refinement statistics for all the crystal structures are summarized in Table 1.

4. Conclusions

Crystallization of soluble proteins can be a very tedious and difficult task that has in part been resolved by automated high-throughput approaches. In this regard, structural genomics/proteomics has contributed immensely by introducing improved and novel technologies that are feeding the field of protein crystallography. High-throughput techniques have resulted in an abundance of new protein structures and in some cases their functions are still unknown. Such data does not contribute at present to the biological/biochemical understanding of the corresponding functions of these proteins, which remains the main incentive for the elucidation of three-dimensional biomacromolecular structures. A biological or biochemical question promotes the structural study of the molecular system. The mechanistic question of intrinsically active p38α MAP kinase variants motivated the study described above. Based on previously available data on p38α, the crystallization of these variants should have been straightforward, yet we were proven wrong. Since these mutants are intrinsically active, they were obtained with a nonhomogeneous phosphorylation pattern when expressed at 303–310 K. This was initially discovered during the unfruitful automated crystallization assays. Only after an extensive analysis of the protein were we able to abolish phosporylation completely by reducing both the temperature and duration of induction. In addition, the N-terminal hexahistidine spacer was significantly shortened. These alterations facilitated the growth of well diffracting crystals, the structures of which were subsequently solved. Such projects necessitate close attention in order to succeed and only the low-throughput approaches that have partially been described above led to success.

This work was supported by Israeli Science Foundation (ISF) grant 495-03 (to OL) and by funds from the Altertum Elsa and Elyahu Pen Foundations (to OL and DE). We thank the staff of the ESRF, Grenoble, France for their helpful assistance.

References

Askari, N., Diskin, R., Avitzour, M., Capone, R., Livnah, O. & Engelberg, D. (2007). In the press.
Avitzour, M., Diskin, R., Raboy, B., Askari, N., Engelberg, D. & Livnah, O. (2007). In the press.
Berman, H. M., Battistuz, T., Bhat, T. N., Bluhm, W. F., Bourne, P. E., Burkhardt, K., Feng, Z., Gilliland, G. L., Iype, L., Jain, S., Fagan, P., Marvin, J., Padilla, D., Ravichandran, V., Schneider, B., Thanki, N., Weissig, H., Westbrook, J. D. & Zardecki, C. (2002). *Acta Cryst.* D**58**, 899–907.
Bucher, M. H., Evdokimov, A. G. & Waugh, D. S. (2002). *Acta Cryst.* D**58**, 392–397.
Bukhtiyarova, M., Northrop, K., Chai, X., Casper, D., Karpusas, M. & Springman, E. (2004). *Protein Expr. Purif.* **37**, 154–161.
Canagarajah, B. J., Khokhlatchev, A., Cobb, M. H. & Goldsmith, E. J. (1997). *Cell*, **90**, 859–869.
Cano, E. & Mahadevan, L. C. (1995). *Trends Biochem. Sci.* **20**, 117–122.
Cobb, M. H. & Goldsmith, E. J. (2000). *Trends Biochem. Sci.* **25**, 7–9.
Diskin, R., Askari, N., Capone, R., Engelberg, D. & Livnah, O. (2004). *J. Biol. Chem.* **279**, 47040–47049.
Diskin, R., Lebendiker, M., Engelberg, D. & Livnah, O. (2007). *J. Mol. Biol.* **365**, 66–76
Du, P., Loulakis, P., Luo, C., Mistry, A., Simons, S. P., LeMotte, P. K., Rajamohan, F., Rafidi, K., Coleman, K. G., Geoghegan, K. F. & Xie, Z. (2005). *Protein Expr. Purif.* **44**, 121–129.
Durbin, S. D. & Feher, G. (1996). *Annu. Rev. Phys. Chem.* **47**, 171–204.
Engelberg, D. (2004). *Semin. Cancer Biol.* **14**, 271–282.
Jones, T. A., Zou, J.-Y., Cowan, S. W. & Kjeldgaard, M. (1991). *Acta Cryst.* A**47**, 110–119.
Lee, J. C., Kumar, S., Griswold, D. E., Underwood, D. C., Votta, B. J. & Adams, J. L. (2000). *Immunopharmacology*, **47**, 185–201.
Morris, R. J., Perrakis, A. & Lamzin, V. S. (2003). *Methods Enzymol.* **374**, 229–244.
Murshudov, G. N., Vagin, A. A. & Dodson, E. J. (1997). *Acta Cryst.* D**53**, 240–255.
Ono, K. & Han, J. (2000). *Cell Signal.* **12**, 1–13.
Otwinowski, Z. & Minor, W. (1997). *Methods Enzymol.* **276**, 307–326.
Robbins, D. J., Zhen, E., Owaki, H., Vanderbilt, C. A., Ebert, D., Geppert, T. D. & Cobb, M. H. (1993). *J. Biol. Chem.* **268**, 5097–5106.
Songyang, Z., Lu, K. P., Kwon, Y. T., Tsai, L. H., Filhol, O., Cochet, C., Brickey, D. A., Soderling, T. R., Bartleson, C., Graves, D. J., DeMaggio, A. J., Hoekstra, M. F., Blenis, J., Hunter, T. & Cantley, L. C. (1996). *Mol. Cell. Biol.* **16**, 6486–6493.
Stura, E. A., Chen, P., Wilmot, C. M., Arevalo, J. H. & Wilson, I. A. (1992). *Proteins*, **12**, 24–30.
Stura, E. A. & Wilson, I. A. (1991). *J. Cryst. Growth*, **110**, 270–282.
Vagin, A. A. & Isupov, M. N. (2001). *Acta Cryst.* D**57**, 1451–1456.
Wang, Z., Harkins, P. C., Ulevitch, R. J., Han, J., Cobb, M. H. & Goldsmith, E. J. (1997). *Proc. Natl Acad. Sci. USA*, **94**, 2327–2332.
Wilson, K. P., Fitzgibbon, M. J., Caron, P. R., Griffith, J. P., Chen, W., McCaffrey, P. G., Chambers, S. P. & Su, M. S. (1996). *J. Biol. Chem.* **271**, 27696–27700.
Zarubin, T. & Han, J. (2005). *Cell Res.* **15**, 11–18.